J. Fluid Mech. (1979), *vol.* 94, *part* 2, *pp.* 383–400
Printed in Great Britain

Turbulent flow and heat transfer in pipes with buoyancy effects

By A. M. ABDELMEGUID AND D. B. SPALDING

Imperial College of Science and Technology, Mechanical Engineering Department, Exhibition Road, London SW7 2BX

(Received 4 November 1977 and in revised form 8 December 1978)

A finite-difference procedure is employed to predict the turbulent flow and heat transfer in horizontal, inclined and vertical pipes when influenced by buoyancy. The flow is treated as parabolic; and the turbulence model used involves the solution of two differential equations, one for the kinetic energy of turbulence and the other for its dissipation rate. Results are presented for the velocity and temperature fields, and the associated flow-resistance and heat-transfer coefficients. The predictions for horizontal and vertical pipes have been compared with the available experimental results, and the agreement obtained is good.

CONTENTS

0022–1120/79/4245–7520 $02.00

1. Introduction

1.1. *The problem considered*

The flow and heat-transfer characteristics of turbulent pipe flow are affected by the presence of gravity forces; at moderate Reynolds numbers and high Grashof numbers, there occur considerable distortion of velocity and temperature profiles, and changes in the heat-transfer and hydrodynamic resistances. The character of these changes are affected by the inclination of the pipe. For horizontal pipes, the gravity force is perpendicular to the main flow direction and operates on the cross-stream flow; then the flow is three-dimensional. For vertical pipes, the gravity force is aligned with the pipe axis, so that axial symmetry is preserved. For inclined pipes, the gravity force acts in both the main-flow and the cross-stream-flow directions.

The present paper demonstrates and tests a means of computing the velocity and temperature fields, and the associated flow-resistance and heat-transfer coefficients, in pipe flows with appreciable buoyancy effects. The situation of fully-developed flow is considered for inclined pipes, while both the developing and fully-developed regions are considered for vertical and horizontal pipes.

1.2. *Previous work*

(*a*) *Horizontal pipes.* The literature on buoyancy-influenced flow and heat transfer in horizontal pipes is limited. Polyakov (1974) presented an analysis for the development of a secondary free-convection current in forced turbulent flow with weak buoyancy, i.e. at low Grashof numbers. In this analysis, he assumed that buoyancy forces do not affect turbulent-transfer coefficients. Skiadaressis & Spalding (1977) presented a finite-difference procedure for the prediction of such flow phenomena, allowing for the associated changes in the turbulent transfer properties; their predictions were in good agreement with experimental data. Petukhov *et al.* (1974) presented experimental data for the local heat transfer, and for the fields of axial velocity and temperature, for air. More recently, an experimental study, also conducted by Petukhov *et al.* (1976), provided data for the distribution of fluctuation intensities of temperature and velocity.

(*b*) *Vertical pipes.* All past theoretical studies on vertical pipes have been confined to the situation of fully-developed flow. Ojalov *et al.* (1967) developed a numerical method for solving the corresponding conservation equations, based on the reduction of the basic conservation laws to three coupled, linear, integro-differential equations. Polyakov (1973) presented a theoretical study of the limits of the influence of the buoyancy forces on the velocity distribution, the temperature, and the heat-transfer and friction resistances.

The measurements of Carr, Connor & Buhr (1973) and Buhr, Horsten & Carr (1974) represent a wide range of data for ascending flow in vertical pipes. They observed that, at high Grashof number, a limiting profile shape was approached, with the centre velocity well below the mean and the maximum occurring in the vicinity of the wall. Petukhov (1976) presented a wide range of experimental data, and concluded that the influence of gravitation on turbulent transfer is determined by two distinct effects: on the one hand, it changes the fields of the average values of velocity and temperature; this results in a change in the turbulent transfer characteristics. On the other hand, it has a direct effect on the motion of the turbulent elements of the fluid, thus strength-

ening or weakening the intensity of turbulent mixing. Depending on the conditions, both effects may be commensurable, or one of them may predominate.

(*c*) *Inclined pipes.* Little research has been done on inclined pipes, and, to the authors' knowledge, none in turbulent flows.

1.3. *Present contribution*

The present paper reports the results of a theoretical analysis of fluid flow and heat transfer in vertical, inclined and horizontal pipes with appreciable influence of buoyancy, and with uniform heat transfer through the walls.

The aims of the present work are to extend and generalize the numerical method used by Skiadaressis & Spalding (1977) to inclined pipes, and so to provide insight into the physical processes involved, while simultaneously demonstrating the capabilities of the calculation procedure as a useful design tool.

The main assumption is that downstream effects are not transmitted upstream; the assumption renders the finite-difference procedure fully parabolic. The numerical algorithm employed is that reported by Patankar & Spalding (1972); the effects of turbulence are represented by a 'two-equation model' (Launder & Spalding 1974), in which differential equations are solved for the turbulence energy and for its dissipation rate. The velocity and temperature fields, as well as the heat-transfer and flow-resistance coefficients, have been predicted both in the developing and the fully-developed regions, and for both vertical and horizontal pipes. Comparisons with experimental data for fully-developed longitudinal-velocity and temperature profiles, are presented for horizontal and vertical pipes. Comparison of heat-transfer coefficients with experimental data are presented also for horizontal pipes.

2. Prediction procedure

2.1. *Governing differential equations*

The equations governing the present problem are those of continuity, momentum and energy. These equations, in cylindrical-polar co-ordinates, and in accordance with figure 1, take the following forms.

Continuity:

$$\frac{1}{r}\frac{\partial}{\partial r}(\rho r v)+\frac{1}{r}\frac{\partial}{\partial \theta}(\rho u)+\frac{\partial}{\partial z}(\rho w)=0. \tag{2.1}$$

Longitudinal momentum:

$$\frac{1}{r}\frac{\partial}{\partial r}(\rho r v w)+\frac{1}{r}\frac{\partial}{\partial \theta}(\rho u w)+\frac{\partial}{\partial z}(\rho w^2) = -\frac{\partial \bar{p}}{\partial z}-\rho g\beta(T-T_{\mathrm{ref}})\sin\alpha+\frac{1}{r}\left[\frac{\partial}{\partial r}(r\tau_{rz})+\frac{\partial \tau_{\theta z}}{\partial \theta}\right]. \tag{2.2}$$

Radial momentum:

$$\frac{1}{r}\frac{\partial}{\partial r}(\rho r v^2)+\frac{1}{r}\frac{\partial}{\partial \theta}(\rho v u)+\frac{\partial}{\partial z}(\rho w v)-\frac{\rho u^2}{r} = -\frac{\partial p}{\partial r}-\rho g\beta(T-T_{\mathrm{ref}})\cos\theta\cos\alpha+\frac{1}{r}\left[\frac{\partial}{\partial r}(r\tau_{rr})+\frac{\partial}{\partial \theta}(\tau_{r\theta})\right]-\frac{\tau_{\theta\theta}}{r}. \tag{2.3}$$

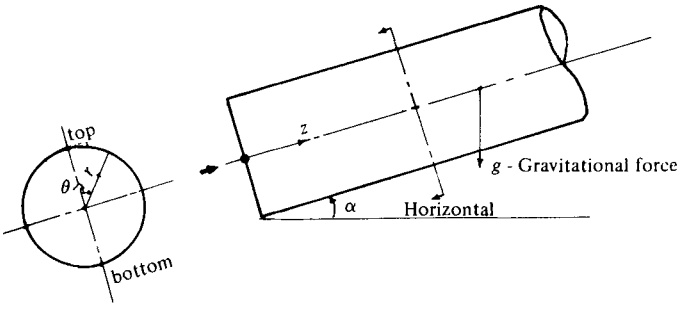

FIGURE 1. The geometry considered.

Angular momentum:

$$\frac{1}{r}\frac{\partial}{\partial r}(\rho r v u)+\frac{1}{r}\frac{\partial}{\partial \theta}(\rho u^2)+\frac{\partial}{\partial z}(\rho w u)+\frac{\rho u v}{r}$$

$$=-\frac{1}{r}\frac{\partial p}{\partial \theta}+\rho g\beta(T-T_{\text{ref}})\sin\theta\cos\alpha+\frac{1}{r}\left[\frac{1}{r}\frac{\partial}{\partial r}(r^2\tau_{r\theta})+\frac{\partial \tau_{\theta\theta}}{\partial \theta}\right]. \tag{2.4}$$

Thermal energy:

$$\frac{1}{r}\frac{\partial}{\partial r}(\rho r v T)+\frac{1}{r}\frac{\partial}{\partial \theta}(\rho u T)+\frac{\partial}{\partial z}(\rho w T)=\frac{1}{r}\left[\frac{\partial}{\partial r}(r J_r)+\frac{\partial}{\partial \theta}(J_\theta)\right]. \tag{2.5}$$

In these equations u, v and w represent the velocity components in the θ, r and z co-ordinate directions respectively. θ is measured from the top of the pipe. ρ represents the density, p is the pressure and β is the thermal expansion coefficient. The τ's represent components of the shear-stress tensor and are expressible in terms of the velocity gradients and an effective viscosity, which varies in the field. J's represent components of heat-flux and are expressible in terms of the temperature gradients and an effective heat diffusivity.

The above equations have been reduced from the general three-dimensional form to that shown by use of the assumptions stated below:

(i) The flow is assumed to be of the boundary-layer type. This implies that neither momentum nor heat is transferred by molecular or turbulent mixing in the longitudinal direction.

(ii) A space-average pressure, $\overline{p}$, is supposed to prevail at each cross-section in the longitudinal momentum equation; whereas the pressure variations with r and θ are allowed to influence the other two momentum equations. This 'pressure uncoupling' is a necessity, legitimate for parabolic flows, if a marching-integration procedure is to be used.

(iii) The viscous dissipation is omitted from the energy equation, because the velocities in question are low.

(iv) Only small variations in density occur, due to temperature differences; and the Boussinesq approximation prevails. In (2.5), T_{ref} represents a reference temperature in the field.

2.2. *Turbulence model*

The effective viscosity, μ_{eff}, is calculated from a two-equation turbulence model (Launder & Spalding 1974). The governing differential equations for turbulent kinetic energy k and its dissipation rate ϵ are:

Kinetic energy of turbulence,

$$\frac{1}{r}\frac{\partial}{\partial r}(\rho rvk)+\frac{1}{r}\frac{\partial}{\partial \theta}(\rho uk)+\frac{\partial}{\partial z}(\rho wk)=\frac{1}{r}\frac{\partial}{\partial r}\left[r\Gamma_k\frac{\partial k}{\partial r}\right]+\frac{1}{r^2}\frac{\partial}{\partial \theta}\left[\Gamma_k\frac{\partial k}{\partial \theta}\right]+G-\rho\epsilon; \tag{2.6}$$

Dissipation rate,

$$\frac{1}{r}\frac{\partial}{\partial r}(\rho rv\epsilon)+\frac{1}{r}\frac{\partial}{\partial \theta}(\rho u\epsilon)+\frac{\partial}{\partial z}(\rho w\epsilon)=\frac{1}{r}\frac{\partial}{\partial r}\left[r\Gamma_\epsilon\frac{\partial \epsilon}{\partial r}\right]+\frac{1}{r^2}\frac{\partial}{\partial \theta}\left[\Gamma_\epsilon\frac{\partial \epsilon}{\partial \theta}\right]+C_1\frac{G\epsilon}{k}-C_2\frac{\rho\epsilon^2}{k}; \tag{2.7}$$

where

$$G\equiv\mu_t\left[2\left\{\left(\frac{1}{r}\frac{\partial u}{\partial \theta}+\frac{v}{r}\right)^2+\left(\frac{\partial v}{\partial r}\right)^2\right\}+\left\{r\frac{\partial}{\partial r}\left(\frac{u}{r}\right)+\frac{1}{r}\frac{\partial v}{\partial \theta}\right\}^2+\left\{\frac{\partial w}{\partial r}\right\}^2+\left\{\frac{1}{r}\frac{\partial w}{\partial \theta}\right\}^2\right]. \tag{2.8}$$

The expression for μ_{eff} is

$$\mu_{\text{eff}}=\mu_{\text{laminar}}+C_\mu\rho k^2/\epsilon. \tag{2.9}$$

The turbulent viscosity μ_t is calculated from the relationship

$$\mu_t=C_\mu\rho k^2/\epsilon. \tag{2.10}$$

The model contains five empirical constants which are assigned the following commonly used values:

$$C_\mu=0{\cdot}09,\quad C_1=1{\cdot}44,\quad C_2=1{\cdot}92,\quad Pr_k=1{\cdot}0,\quad Pr_\epsilon=1{\cdot}3.$$

A special but conventional treatment is adopted for the near-wall regions, since the variations of the flow properties are much steeper in this region; the practices adopted here are the same as described by Launder & Spalding (1974), with appropriate extensions to account for the three-dimensional nature of the flow. No special terms are included in the equations for k and ϵ to account for the interaction of buoyancy and turbulence, despite the conclusion of Petukhov (1976) mentioned above. Computational tests showed that the inclusion of these terms has no significant effect on flow or heat transfer.

2.3. *Solution procedure*

A finite-difference forward-marching procedure is applied to solve the equations governing the flow and heat transfer. The finite-difference equations are solved by marching from an upstream station, where the flow conditions are known, to successive stations downstream. The procedure thus computes the flow section by section along the pipe length. A full account of the procedure is given by Patankar & Spalding (1972), its main feature is that the downstream pressure field is first guessed, so as to lead to a preliminary velocity field, satisfying the momentum equations but not the continuity equation, then corrections are made in a systematic manner until *all* the equations are satisfied. No modifications were needed or made to the solution procedure.

2.4. *Computational details*

(*a*) *The computer program.* The differential equations described in § 2.1, together with the Patankar–Spalding (1972) method, were embodied in the computer code STABLER (*Steady Three-dimensional Analysis of Boundary-Layer Equations Revised*).

(*b*) *The grid.* Two different types of grid were used. For inclined and horizontal pipes, for which the flow is symmetrical about a vertical plane, computation was confined to half of the pipe. A grid of 15 nodes in the radial direction and 11 nodes in the angular

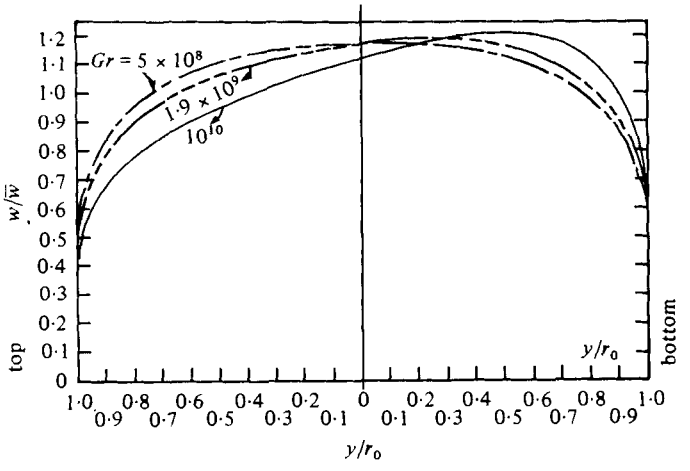

FIGURE 2. The variation of the fully developed velocity profile with heat input in horizontal pipes (view in vertical-diametral plane; $Re = 49\,500$, r_0 is the pipe radius).

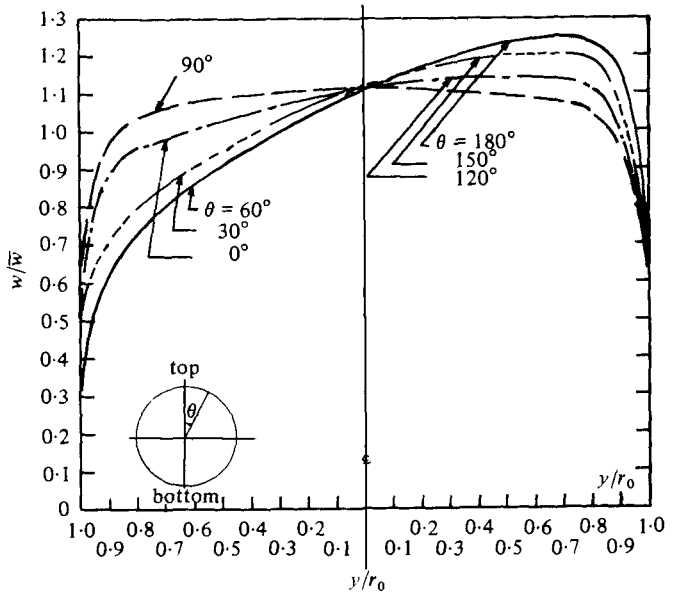

FIGURE 3. Fully developed velocity profiles at different angular stations in horizontal pipes under considerable thermo-gravitational forces ($Re = 25\,000$, $Gr = 10^{10}$).

direction was employed. In the angular direction, a nearly uniform grid distribution was chosen; in the radial direction, more grid nodes were concentrated in the region close to the wall.

For vertical pipes, the flow was axisymmetric and fewer grid nodes were needed in the circumferential direction. A 15×6 grid was employed, but, strictly speaking, a 15×1 grid was all that was needed.

(c) *Computational cost.* An initial isothermal section of 20 diameters preceded the test section in all the predictions.

Approximately 400 sections were visited by the marching-integration process, in the passage from entry to full development. The computer time on a CDC 6600 computer was of the order of 0·5 seconds per forward step.

3. Results and discussion

3.1. *Horizontal pipes*

Velocity profiles. Figure 2 presents fully developed longitudinal-velocity profiles, at a fixed angular position and at various Grashof numbers Gr. Figure 3 shows such profiles at various angular positions, for a fixed Gr.

The development of the longitudinal-velocity contours with distance from the entry, at a typical Gr, is shown in figure 4.

Figure 5 presents a comparison of the predicted velocity profiles in the vertical and horizontal diametral planes, with experimental data by Petukhov *et al.* (1974), and Petukhov (1976).

Temperature profiles. The temperature distributions in the cross-stream plane, are presented in figure 6. The figure also presents, for comparison, experimental data by Petukhov *et al.* (1974) and Petukhov (1976).

In figure 7, the development of Nusselt number, Nu, is plotted with distance from the entry, at Gr equal $1{\cdot}9 \times 10^9$ at the top and bottom pipe generators. The figure also presents a comparison with the experimental data by Petukhov *et al.* (1974).

Discussion. It can be seen from figures 2 and 6 that the longitudinal-velocity and temperature maximums are shifted from the centre-line, because of the increase in Gr. Figures 5, 6 and 7 show that the agreement between measurements and predictions is good.

3.2. *Vertical pipes*

(*a*) *Ascending flow.* Figure 8 presents the development of the longitudinal-velocity profile with distance from the entry, at a fixed Grashof number. Figures 9 and 10 present the fully developed longitudinal-velocity and turbulent-kinetic-energy profiles, for various Grashof numbers. Figure 11 presents the variation of friction factor, with Gr for constant Re; f_t represents the friction factor for turbulent forced flow.

Figure 12 presents the fully-developed temperature profiles for various Gr. In figure 13, the variation of Nu at various Gr is presented.

It can be seen from figures 9 and 10 that the mean flow and the turbulent transfer are much affected by the value of Gr: for Gr less than a critical value, Gr_c (here 10^9), the effect of buoyancy on turbulence characteristics is modest, and its effect on the averaged flow can be neglected; for Gr greater than Gr_c, buoyancy affects both the averaged flow and the turbulent transfer.

Figure 9 shows also that the maximum velocity occurs in the vicinity of the wall; and, with increase of Gr, the maximum velocity near the wall increases in value and is located nearer to the wall. This is the same trend as is described by Carr *et al.* (1973).

It can also be seen from figure 10 that the turbulent kinetic energy decreases with increase of Gr, until Gr_c is reached, and then increases; and it can be seen from

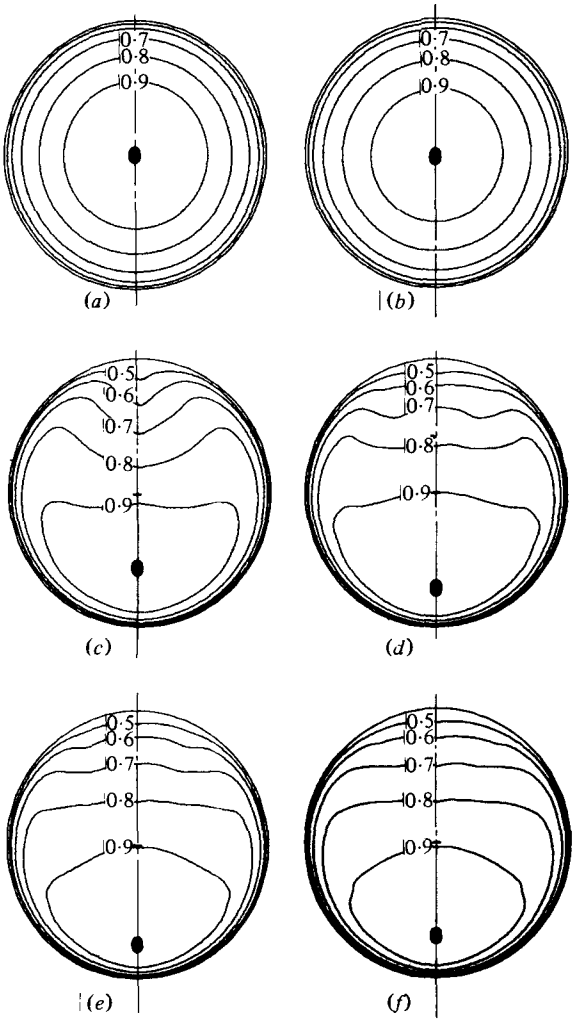

FIGURE 4. Axial-velocity contours in the thermal entry length in a horizontal pipe under considerable thermo-gravitational forces ($Re = 25000$, $Gr = 10^{10}$; contours are for w/w_{max}). (*a*) At the start of heating. (*b*) $z/D = 2{\cdot}4$. (*c*) $z/D = 13{\cdot}75$. (*d*) $z/D = 25{\cdot}74$. (*e*) $z/D = 37{\cdot}75$. (*f*) Fully developed, $z/D = 49{\cdot}75$.

figure 13, that, at first, the Nusselt number decreases when the heat input is increased, and then rises. The initial decrease in Nu accords with the initial decrease in the turbulent kinetic energy; the subsequent increase in Nu is due to the buoyancy forces becoming dominant on both the averaged flow and the turbulent transfer.

Figures 14 and 15 compare the predictions with the experimental data of Buhr *et al.* (1974), with mercury as a working fluid. In the predictions, special attention had to be given to the so-called 'wall function'; the treatment adopted was that of El Hadidy & Spalding (1978, unpublished work). Agreement between measurements and predictions is satisfactory.

(*b*) *Descending flow.* Figures 16 and 17 present the fully developed longitudinal-velocity and turbulent-kinetic-energy profiles for various Grashof numbers. Figure

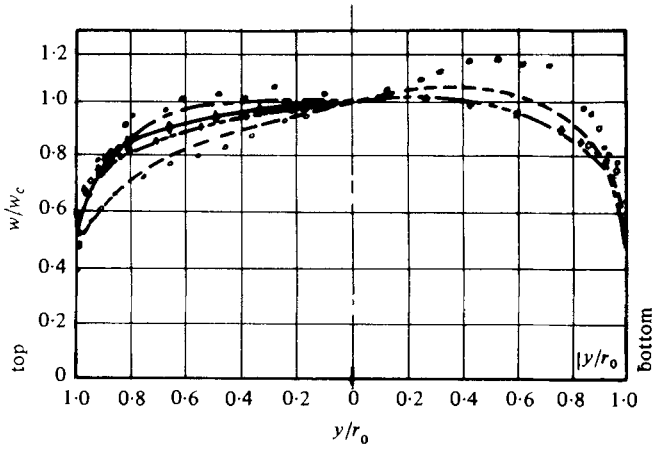

FIGURE 5. Velocity profiles compared with Petukhov *et al.* (1974) and Petukhov (1976). (Predicted, experimental) results for the vertical-diametral plane: (——·——, ◇), $Re = 52000$, $Gr = 10^9$; (– – – –, ○), $Re = 26000$, $Gr = 7{\cdot}7 \times 10^8$. Results for the horizontal-diametral plane: (——, ◆), $Re = 52000$, $Gr = 10^9$; (—·—, ●), $Re = 26000$, $Gr = 7{\cdot}7 \times 10^8$.

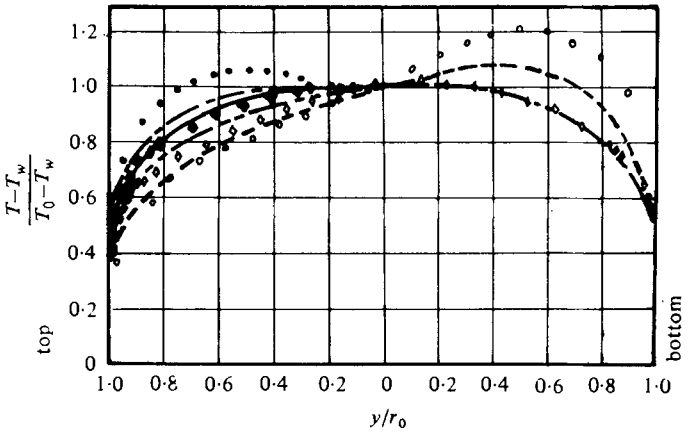

FIGURE 6. Temperature profiles compared with the data of Petukhov *et al.* (1974). Symbols as in figure 5.

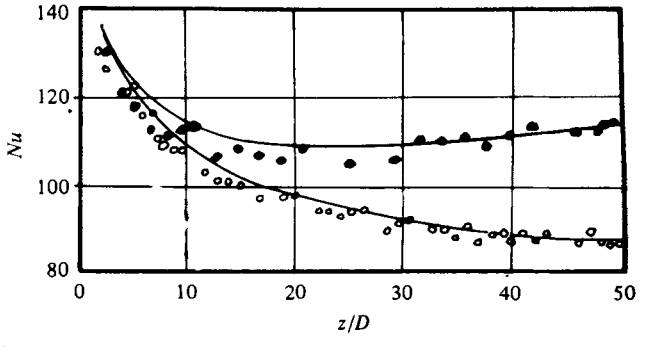

FIGURE 7. Variation of Nusselt number in the thermal entry length compared with the data of Petukhov *et al.* (1974). ($Re = 25000$, $Gr = 10^{10}$.) Experimental: ○, $\theta = 0°$; ●, $\theta = 180°$. Predicted: ——.

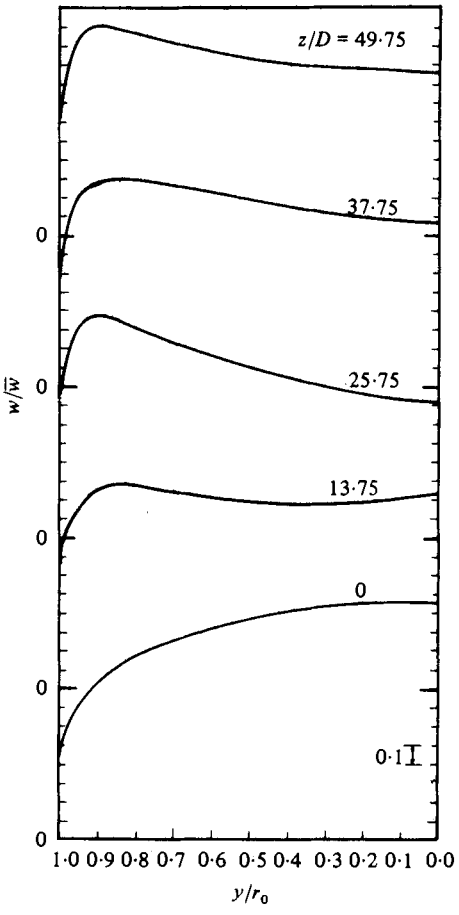

FIGURE 8. Axial-velocity profiles in the thermal entry length for an ascending flow of air in a vertical pipe ($Re = 25000$, $Gr = 10^{10}$).

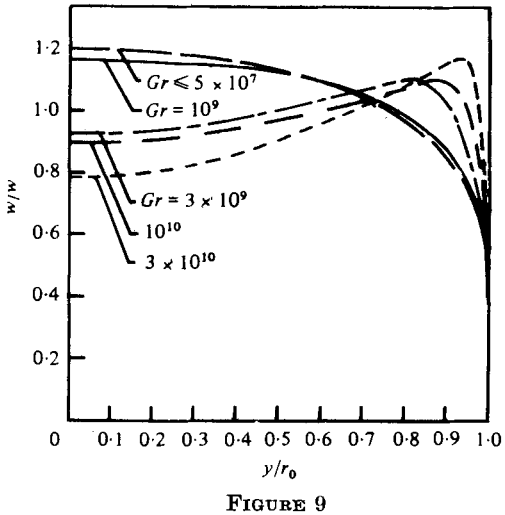

FIGURE 9

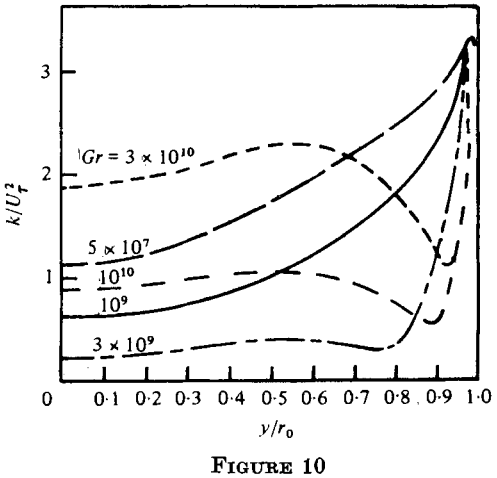

FIGURE 10

FIGURE 9. Variation of axial-velocity profile with the heat input for an ascending air in a vertical pipe ($Re = 25000$).

FIGURE 10. Variation of the kinetic energy of turbulence with the heat input ($Re = 25000$).

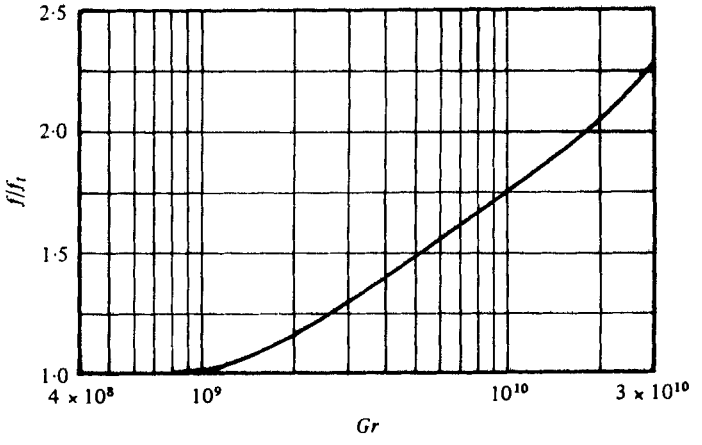

FIGURE 11. Friction factor variation with heat input (ascending flow).

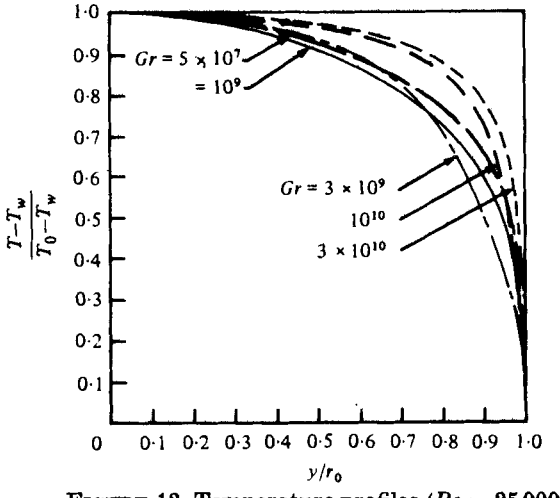

FIGURE 12. Temperature profiles (Re = 25 000).

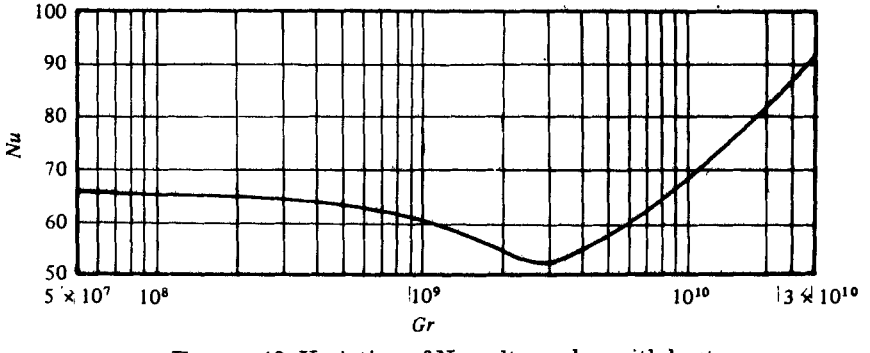

FIGURE 13. Variation of Nusselt number with heat input (Re = 25 000, ascending flow).

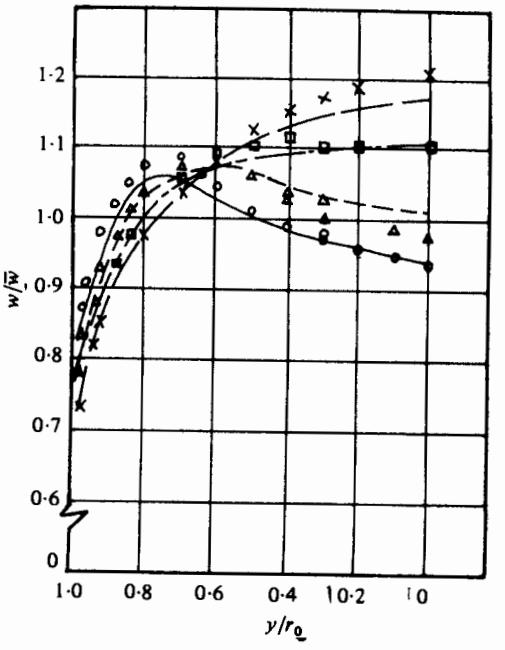

FIGURE 14. Comparison with the data of Buhr *et al.* (1974) of velocity profiles. (Experimental, predicted) results: (×, — —), $Re = 60\,600$, $Gr = 1{\cdot}19 \times 10^8$; (□, —·—), $Re = 62\,200$, $Gr = 5{\cdot}88 \times 10^8$; (△, – – – –), $Re = 65\,400$, $Gr = 8{\cdot}87 \times 10^8$; (○, ——), $Re = 63\,200$, $Gr = 1{\cdot}61 \times 10^9$.

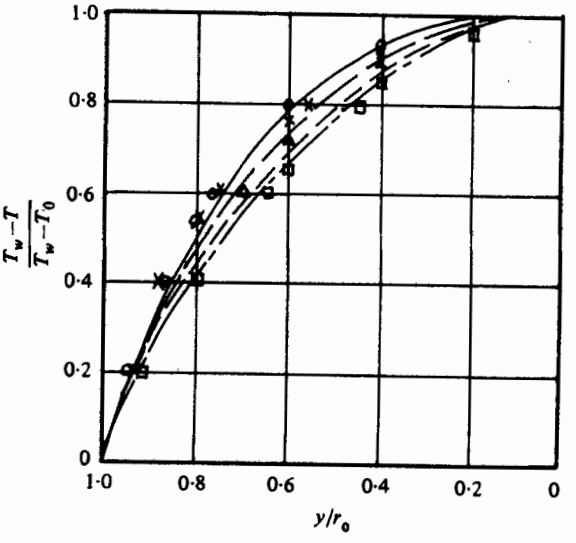

FIGURE 15. Comparison with the data of Buhr *et al.* (1974) of temperature profiles. (Experimental, predicted) results: (×, — —), $Re = 61\,000$, $Gr = 1{\cdot}11 \times 10^8$; (□, —·—), $Re = 61\,600$, $Gr = 5{\cdot}88 \times 10^8$; (△, – – – –), $Re = 62\,400$, $Gr = 8{\cdot}76 \times 10^8$; (○, ——), $Re = 65\,000$, $Gr = 1{\cdot}63 \times 10^9$.

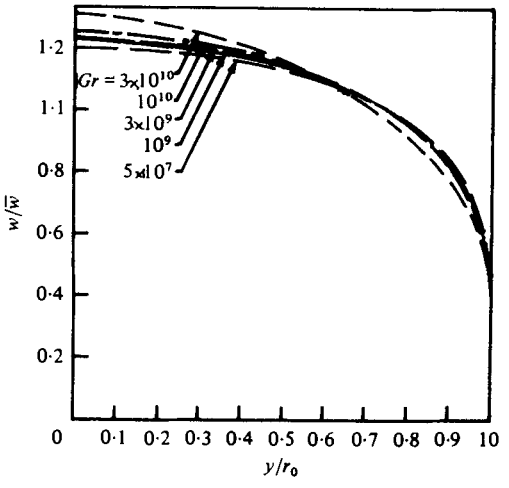

FIGURE 16

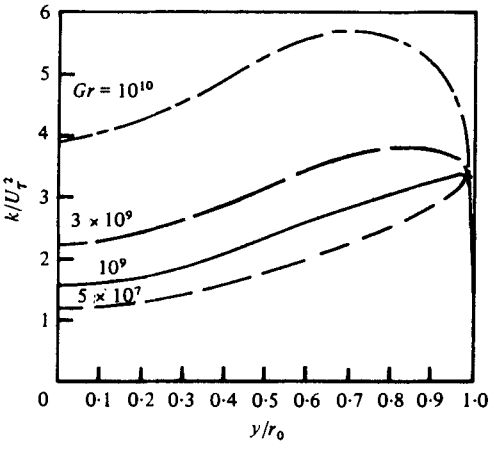

FIGURE 17

FIGURE 16. Variation of axial-velocity profile with heat input for a descending air in a vertical pipe.

FIGURE 17. Variation of the kinetic energy of turbulence with heat input.

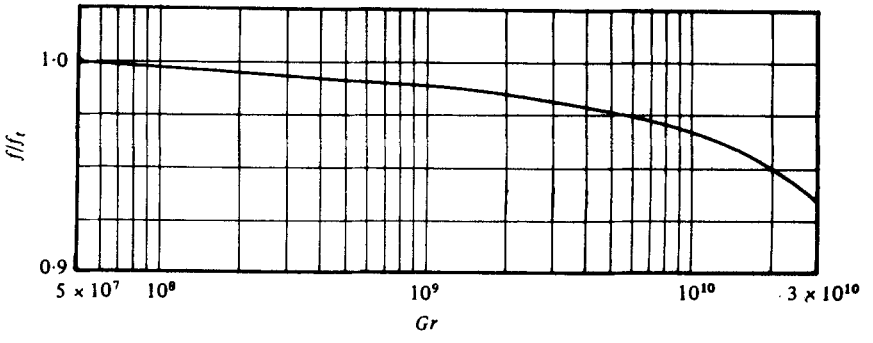

FIGURE 18. Variation of friction with heat input in a descending flow of air (Re = 25000).

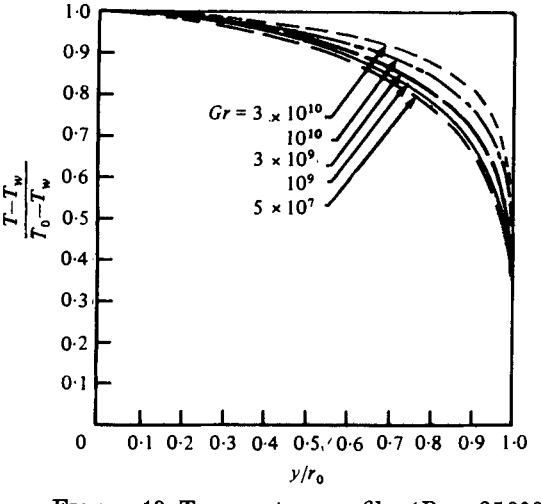

FIGURE 19. Temperature profiles (Re = 25000).

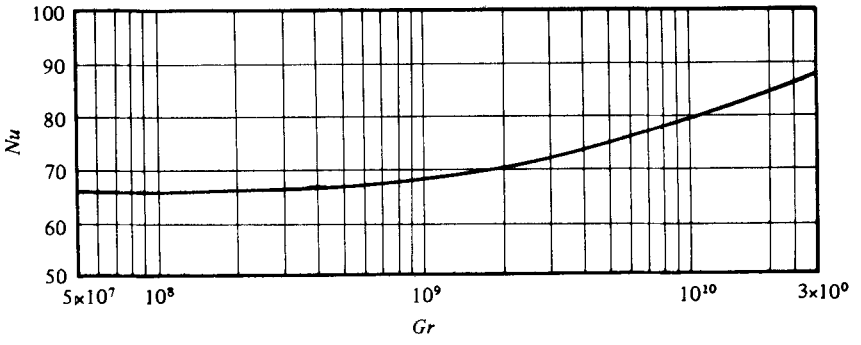

FIGURE 20. Variation of Nusselt number with heat input in a descending flow of air (Re = 25000).

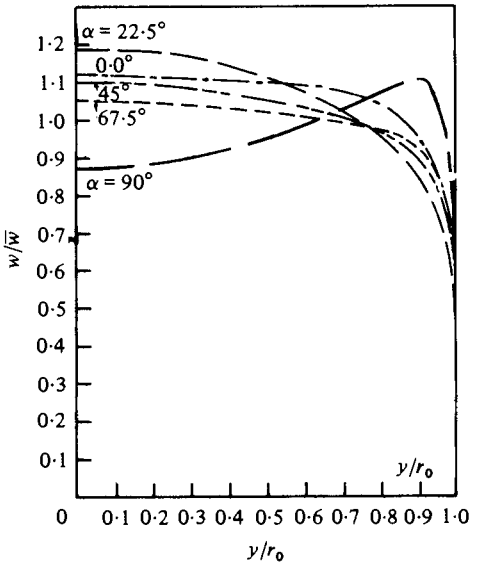

FIGURE 21. Variation of axial-velocity profile with the tube inclination angle (view in the inclined diametral plane; Re = 25000, Gr = 10^{10}).

18 presents the variation of friction factor, with Gr, for constant Re. Figure 19 shows the fully-developed temperature profiles at various Gr; figure 20 presents the variation of Nu with Gr. It can be seen from figure 16 that the maximum velocity increases with the increase in Gr, and the velocity profile becomes fuller. It can also be seen that the influence of buoyancy on the turbulent transfer considerably exceeds its effect on the averaged flow. No experimental data are available for verification of these predictions.

3.3. *Inclined pipes*

The predictions made for inclined pipes are for a fully developed, ascending flow at Re = 25000, Gr = 10^{10}. No experimental data are available for comparison.

Figure 21 presents the variation of the longitudinal-velocity profiles, in the inclined diametral plane, with pipe-inclination angle. Figure 22 presents the corresponding longitudinal-velocity profiles in the vertical diametral plane. Figure 23 shows the

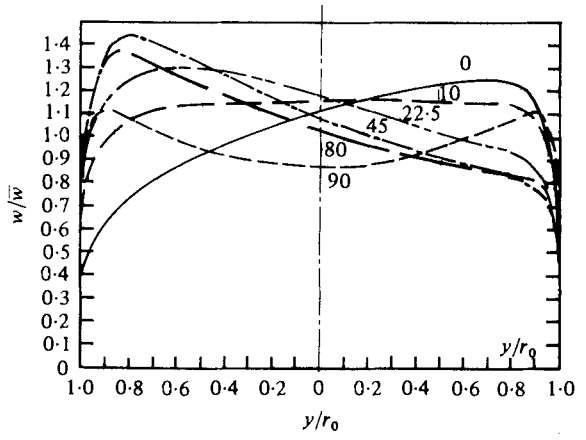

FIGURE 22. Variation of the axial-velocity profiles with the tube inclination angles (view in the vertical-diametral plane; $Gr = 10^{10}$, $Re = 25000$).

variation of the corresponding longitudinal-velocity contours. Figure 24 presents the distributions of Nu on the pipe periphery, at various tube-inclination angles. Figure 25 presents the variation of the average Nu number, based on the average wall temperature, at various tube angles. It can be seen that there exists an inclination angle for which the averaged Nu number has a maximum value.

4. Conclusions

Numerical predictions of flow and heat transfer in horizontal, inclined and vertical pipes with appreciable buoyancy influences, and with uniform heat flux at the wall, have been performed by means of a finite-difference forward-marching procedure. The following were found to be true.

(*a*) *For horizontal pipes:*

(i) The longitudinal velocity maximum shifts towards the pipe bottom to an extent which increases with Grashof number.

(ii) The results are in agreement with available measurements.

(*b*) *For vertical pipes:*

(1) *Ascending flow*

(i) For Gr less than some critical value, Gr_c, the effect of buoyancy on turbulence is modest; and its effect on the averaged flow can be neglected.

(ii) For Gr greater than Gr_c, the buoyancy forces affect both the averaged flow and the turbulent transfer.

(iii) For Gr greater than Gr_c, a minimum velocity occurs at the centre-line of the pipe, and a maximum velocity occurs somewhere between the wall and the pipe axis; with increase of Gr the minimum velocity located at the centre-line decreases, and the maximum velocity near the wall increases and approaches the wall.

(iv) The Nusselt number decreases first with an increase in Gr until Gr_c is reached; then it starts to increase monotonically.

(v) The results are in good agreement with available measurements.

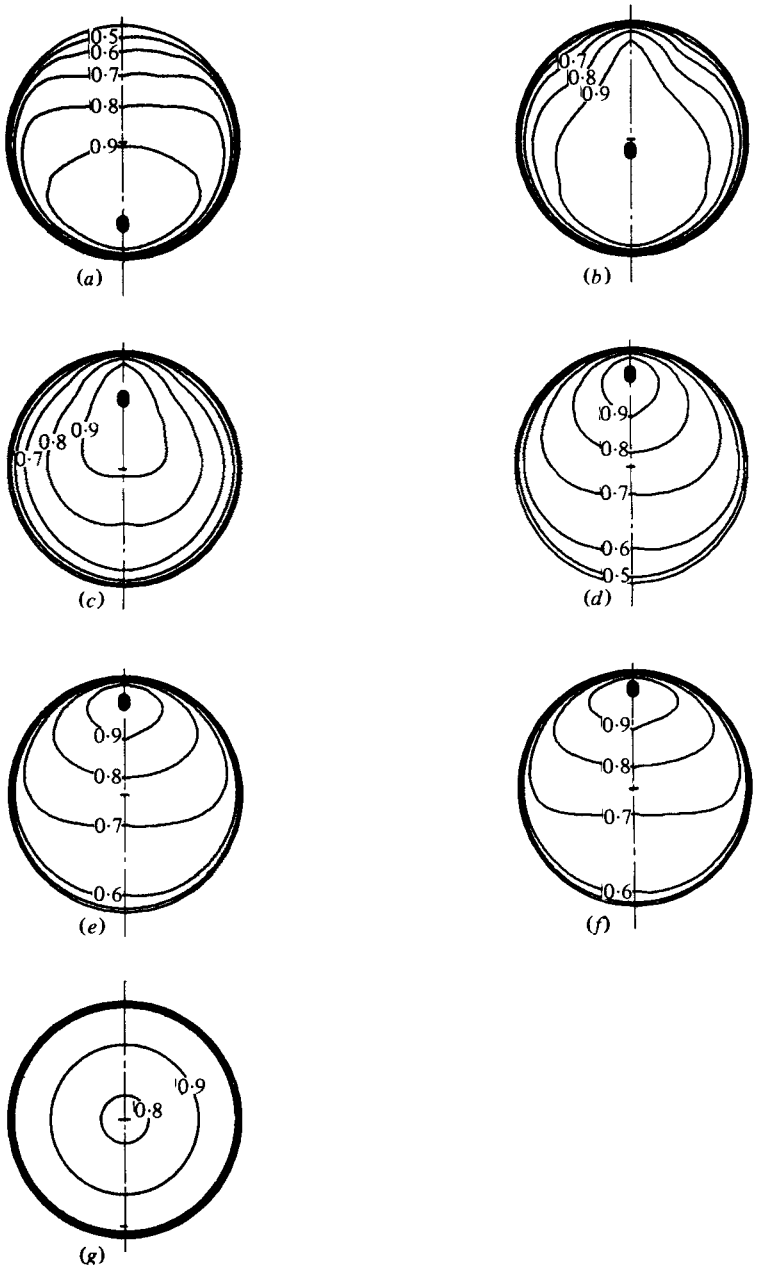

FIGURE 23. The variation of axial-velocity contours with pipe inclination (ascending flow; $Gr = 10^{10}$, $Re = 25\,000$). (*a*) $\alpha = 0°$, horizontal. (*b*) $\alpha = 10°$. (*c*) $\alpha = 22{\cdot}5°$. (*d*) $\alpha = 45°$. (*e*) $\alpha = 67{\cdot}5°$. (*f*) $\alpha = 80°$. (*g*) $\alpha = 90°$, vertical.

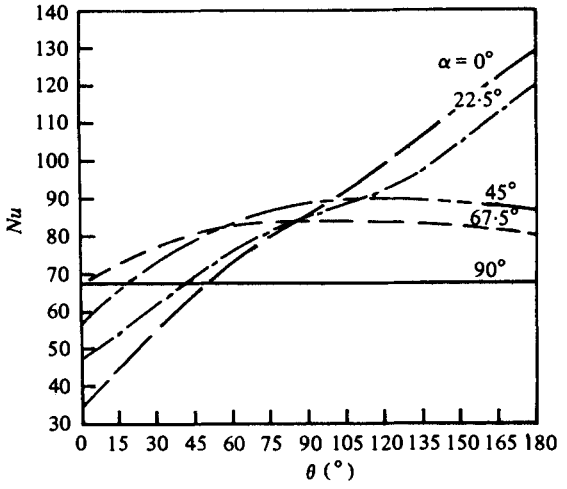

FIGURE 24. Nusselt number distribution on the pipe periphery for different pipe inclination angles ($Re = 25000$, $Gr = 10^{10}$).

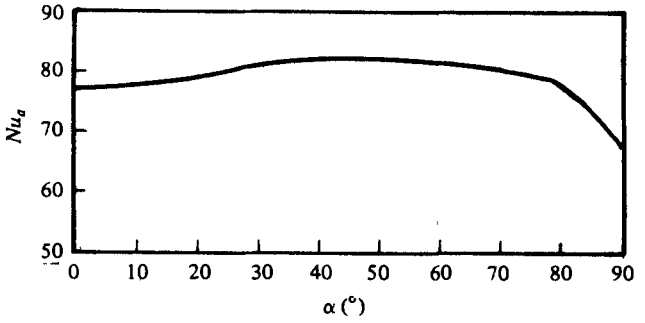

FIGURE 25. Variation of the averaged Nusselt number with the pipe inclination angle ($Re = 25000$, $Gr = 10^{10}$).

(2) *Descending flow*

(i) The maximum velocity increases with the increase in Gr, and the velocity profile becomes more full.

(ii) The influence of buoyancy on the turbulence energy considerably exceeds its effect on the averaged flow.

(3) *Inclined pipes*

(i) At least at the Gr and Re values investigated, there exists an inclination angle for which the averaged Nu has a maximum value.

This work forms a part of the research sponsored by the Science Research Council under grant no. GR/A1 01780. The computer program was loaned by Concentration, Heat and Momentum Limited.

REFERENCES

BUHR, H. O., HORSTEN, E. A. & CARR, A. D. 1974 The distortion of turbulent velocity and temperature profiles on heating for mercury in a vertical pipe. *Trans. A.S.M.E. J. Heat Transfer* **96**, 152.

CARR, A. D., CONNOR, M. A. & BUHR, H. O. 1973 Velocity, temperature and turbulence measurements in air for pipe flow with combined free and forced convection. *Trans. A.S.M.E., J. Heat Transfer* **95**, 445.

LAUNDER, B. E. & SPALDING, D. B. 1974 The numerical computation of turbulent flows. *Comp. Meth. for App. Mech. & Engng* **3**.

OJALOV, M. S., ANAND, D. K. & DUNBAR, R. P. 1967 Combined forced and free turbulent convection in a vertical circular tube with volume heat source and constant wall heat addition. *Trans. A.S.M.E., J. Heat Transfer* **89**, 328.

PATANKAR, S. V. & SPALDING, D. B. 1972 A calculation procedure for heat, mass and momentum transfer in three-dimensional parabolic flows. *Int. J. Heat Mass Transfer* **15**, 1787.

PETUKHOV, B. S. 1976 Turbulent flow and heat transfer in pipes under considerable effect of thermogravitation forces. (Report presented at seminar on Heat Transfer at Turbulent Free Convection.) *Int. Centre Heat & Mass Transfer, Dubrovnik.*

PETUKHOV, B. S., POLYAKOV, A. F., KULESHOV, V. A. & SHECKTER, YU. L. 1974 Turbulent flow and heat transfer in horizontal tubes with substantial influence of thermogravitational forces. *4th Int. Heat Transfer Conf. Tokyo.*

PETUKHOV, B. S., POLYAKOV, A. F., SHECKTER, YU. L. & KULESHOV, V. A. 1976 Experimental study of the effect of thermogravitation upon turbulent flow and heat transfer in horizontal pipes. (Report presented at seminar on Heat Transfer at Turbulent Free Convection.) *International Centre for Heat & Mass Transfer, Dubrovnik.*

POLYAKOV, A. F. 1973 Transient effects due to thermogravity in turbulent and heat transfer. *High Temp.* **11**, 1.

POLYAKOV, A. F. 1974 Development of secondary free-convection currents in forced turbulent flow in horizontal tubes. *J. Appl. Mech. Tech. Phys., PMTF*, **5**.

SKIADARESSIS, D. & SPALDING, D. B. 1977 Prediction of combined free and forced convection in turbulent flow through horizontal pipes. *Lett. Heat & Mass Transfer* **4**, 35.